arXiv:2306.11137v1 [eess.IV] 19 Jun 2023

Deep Learning Framework with Multi-Head Dilated Encoders for Enhanced Segmentation of Cervical Cancer on Multiparametric Magnetic Resonance Imaging

Reza Kalantar[1,2], Sebastian Curcean[2,3], Jessica M Winfield[1,2], Gigin Lin[4], Christina Messiou[1,2], Matthew D Blackledge[1,2,*] and Dow-Mu Koh[1,2]

[1]Department of Radiotherapy and Imaging, the Institute of Cancer Research, London, United Kingdom
[2]Department of Radiology, The Royal Marsden Hospital, London, United Kingdom
[3]Department of Radiation Oncology, Iuliu Hatieganu University of Medicine and Pharmacy, Cluj-Napoca, Romania
[4]Department of Medical Imaging and Intervention, the Chang Gung Memorial Hospital at Linkou and Chang Gung University, Taoyuan, Taiwan
[*]Corresponding author: matthew.blackledge@icr.ac.uk

ABSTRACT

T_2-weighted magnetic resonance imaging (MRI) and diffusion-weighted imaging (DWI) are essential components for cervical cancer diagnosis. However, combining these channels for training deep learning models are challenging due to misalignment of images. Here, we propose a novel multi-head framework that uses dilated convolutions and shared residual connections for separate encoding of multiparametric MRI images. We employ a residual U-Net model as a baseline, and perform a series of architectural experiments to evaluate the tumor segmentation performance based on multiparametric input channels and feature encoding configurations. All experiments were performed using a cohort including 207 patients with locally advanced cervical cancer. Our proposed multi-head model using separate dilated encoding for T_2W MRI, and combined b1000 DWI and apparent diffusion coefficient (ADC) images achieved the best median Dice coefficient similarity (DSC) score, 0.823 (confidence interval (CI), 0.595-0.797), outperforming the conventional multi-channel model, DSC 0.788 (95% CI, 0.568-0.776), although the difference was not statistically significant ($p>0.05$). We investigated channel sensitivity using 3D GRAD-CAM and channel dropout, and highlighted the critical importance of T_2W and ADC channels for accurate tumor segmentations. However, our results showed that b1000 DWI had a minor impact on overall segmentation performance. We demonstrated that the use of separate dilated feature extractors and independent contextual learning improved the model's ability to reduce the boundary effects and distortion of DWI, leading to improved segmentation performance. Our findings can have significant implications for the development of robust and generalizable models that can extend to other multi-modal segmentation applications.

Keywords Deep Learning · Cervical Cancer Segmentation · Multiparametric MRI · Radiology · Radiation Oncology

1 Introduction

Multiparametric magnetic resonance imaging (mpMRI) is a crucial tool in the diagnosis and management of gynecological malignancies, including cervical cancer. It provides detailed anatomical and functional information, which is applied for disease staging, treatment planning, response monitoring, and surveillance for disease recurrence[1, 2, 3]. An important aspect of many mpMRI protocols is diffusion-weighted imaging (DWI), which enhances the contrast and visualization of cellular tumours. DWI is sensitive to the rate of diffusion of water molecules *in vivo*, which is hindered due to increased cell density [4]; the rate of diffusion can be quantified at each spatial location through estimation of maps of apparent diffusion coefficient (ADC). ADC measurements are being increasingly used as a

surrogate biomarker of tumour grade [5, 6], and have shown promising results in identifying early treatment responses, making them desirable for monitoring therapeutic outcomes in cervical cancer [7, 8]. On conventional anatomical T_2-weighted (T_2W) MRI, primary and metastatic tumors exhibit intermediate to high signal intensities, which is used to identify cervical abnormalities, as well as for disease staging and directing MRI-guided interventions [9, 10].

Automating disease detection and delineation on medical images is a critical task, primarily because it aids in extracting valuable biomarkers from images, which enhances clinical decision-making. This process is currently challenged by the requirement for extensive annotated datasets, leading to a high dependency on clinicians and potential inconsistencies due to human contouring variations. Automated tumor segmentation on mpMRI, therefore, holds great significance, not only for reducing the burden on clinicians but also for its potential in improving accuracy and consistency. Furthermore, in contexts such as tumor planning, where manual delineation may not be feasible due to time constraints, these automated methods become particularly indispensable. Therefore, the development of fully automatic tumor segmentation techniques is a crucial step towards achieving more efficient and reliable clinical processes.

The advent of advanced imaging and high-performance technologies has led to a surge of interest in deep learning (DL) and convolutional neural network (CNN)-based approaches for pelvic cancer segmentation [11]. While several studies have explored DL-based segmentation of cervical cancer on MRI [12, 13, 14, 15, 16], there remains a scarcity of research on cancer tumor segmentation utilizing multiparametric MRI. Specifically, few studies have combined semantic knowledge between T_2W MRI and DWI/ADC in this context.

Among related studies, Lin et al. [17] developed a U-Net model for segmenting cervical cancer on DWI and found that multi-channel input (b0, b1000, and ADC) produced the best segmentation performance. However, this study focused on two-dimensional (2D) images and did not incorporate multimodal MRI (e.g. MRI images derived from different sequences). Kano et al. [18] combined 2D and three-dimensional (3D) U-Net models for cervical tumor segmentation on DWI using an ensembling approach. Yoganathan et al. [19] segmented primary tumors along with organs-at-risk (OARs) on T_2W MRI, reporting that integrating segmentations from 2.5D training in axial, coronal, and sagittal planes improved segmentation performance compared with previous 2D models. However, this study was limited to 39 patients and single-channel inputs. Wang et al. [14] proposed a 3D CNN model for cervical tumor segmentation on multimodal MRI, while Hodneland et al. [20] utilized a U-Net with residual connections, employing T_2W MRI, b1000 DWI, and ADC as input channels. However, none of these studies examined the impact of spatial mismatch between multimodal MRI inputs, resulting from distortion in echo-planar imaging (EPI) and soft-tissue deformations between scans [21, 22], on cervical tumor segmentation outcome.

The aim of this study was to develop a novel 3D DL framework that included multi-head dilated residual encoding blocks for combined fine-grained and contextual feature aggregation and training on anisotropic sub-volumes of images, enhancing the segmentation of locally advanced cervical tumors on multiparametric MRI. To our best knowledge, no previous studies have investigated this strategy for automated segmentation of pelvic malignancies.

2 Materials and Methods

2.1 Patient Populations and Imaging Parameters

For this study, a retrospective cohort consisting of 207 patients diagnosed with locally advanced cervical cancer and who underwent pelvic T_2W MRI and DWI on a 3T MAGNETOM TrioTim MRI scanner (Siemens Healthcare, Erlangen, Germany) were selected. The ground truth tumor contours were defined by a clinician with 3 years of experience on T_2W MRI images with the DWI data available for all patients. The acquisition parameters for this dataset are shown

in Table 1. The ADC maps were calculated from DWI images with varying diffusion-weighting magnitude (b-value) (Equation 1), using a mono-exponential fit for two b-values (b0, b1000) (Equation 2) and least-square exponential fit for multiple b-values (b200, b600, b1000) (Equation 3). The Institutional Review Board approved this study, and informed consent was waived (Chang Gung IRB 202000609B0C501).

Table 1: Imaging parameters of the cohort used in this study (n=207). The values are presented as the range from minimum to maximum values, or variables using different protocols within the dataset.

Parameter	**T_2W MRI**	**DWI**
Sequence	Turbo Spin Echo (TSE)	Echo-Planar Imaging (EPI)
Slice Orientation	Axial	Axial
Acquired Matrix Size (read)	224-320	128-172
Reconstructed Matrix Size (read)	256-320	240-248
Reconstructed Pixel Spacing (mm^2)	0.5×0.5-0.8×0.8	1.2×1.2-1.4×1.4
Slice Thickness (mm)	4.0-7.5	4.0-5.0
Flip Angle (°)	90	90
Echo Time (ms)	80-101	60-80
Repetition Time (ms)	3600-8060	3300-10844
Phase Encoding Direction	Anterior Posterior or Left Right	Anterior Posterior
Pixel Bandwidth (Hz/pixel)	190-200	1940-2441
b-values (s/mm^2)	-	[0,1000] or [200,600,1000]

$$S_{b_i} = S_{b_0} \cdot e^{(-b_i D)} \tag{1}$$

$$D = -\frac{1}{b_i} \ln\left(\frac{S_{b_i}}{S_{b_0}}\right) \tag{2}$$

$$D = -\frac{N\sum_{i=1}^{N} b_i \ln(S_{b_i}) - \sum_{i=1}^{N} b_i \sum_{i=1}^{N} ln(S_{b_i})}{N\sum_{i=1}^{N} b_i^2 - (\sum_{i=1}^{N} b_i)^2} \tag{3}$$

where b_i is the b-value, S_{b_0} represents the signal intensity with no diffusion-weighting ($b = 0$), S_{b_i} is the signal intensity at b_i, N is the number of b-values and D denotes the ADC value.

2.2 Network Architectures and Architectural Experiments

In this study, we employed a residual U-Net model, a modified version of conventional U-Net [23], as the benchmark for our segmentation framework. The model architecture was based on an encoder-decoder structure with symmetrical skip connections at each level. Each encoding level consisted of two residual blocks with 3D convolutional layers followed by instance normalization and parametric ReLU activation layer (PReLU). Downsampling was performed in the first convolutional layer (stride=2), and each upsampling block included two residual blocks with 3D strided transposed convolutions and skip connection concatenation layers. The model had four downsampling steps with kernel filters of 32, 64, 128, and 256 and a feature map depth of 512 in the bottleneck. The model was trained on (i) T_2W MRI-only, (ii) T_2W and ADC, and (iii) T_2W, ADC, and b1000 DWI training data, with input channels set to 1, 2, and 3, respectively. Additional details on the model architecture can be found in Figure 1.

To address the boundary effects of DWI in multi-channel training, we conducted a series of architectural experiments. In the first experiment, we replaced the first encoder block in the baseline multi-channel model with three encoding heads. The first head utilized a non-dilated 3D convolutional operation on T_2W MRI inputs only. The other two heads

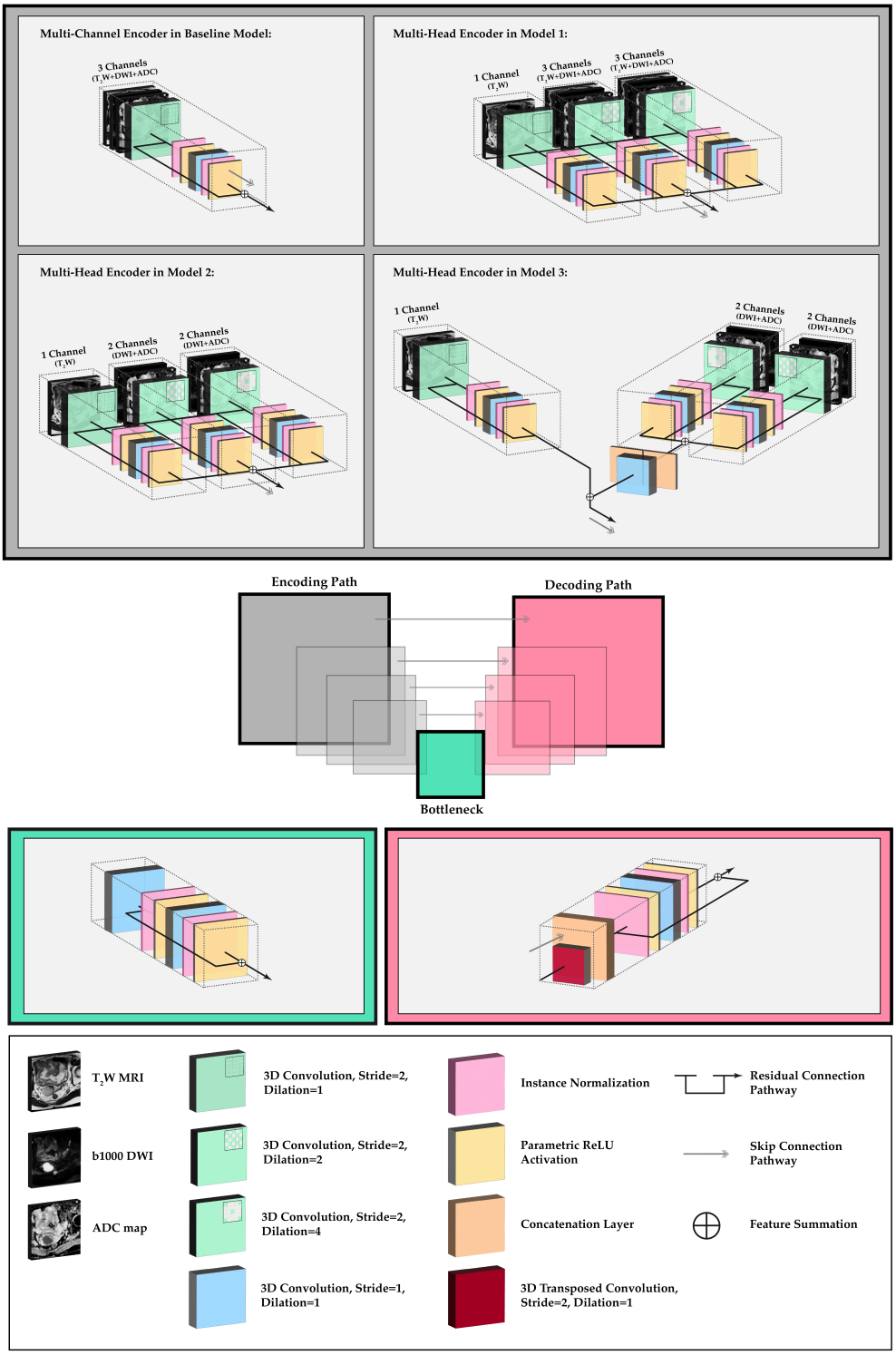

Figure 1: The network topology and the multi-head segmentation training experiments. The operational blocks incorporate residual connections to facilitate the flow of information between different layers. The multi-head models use various encoding and weight-sharing configurations for T_2W MRI and DWI using multiple heads with dilated convolution and connective residual operations.

included 3D convolutions with dilations of 2 and 4 respectively, accepting three input channels: T_2W , b1000 DWI and ADC. These heads were connected by residual weight sharing and feature activation summation nodes, see Figure 1 (multi-head model 1).

In the second multi-head model, we utilized separate encoding of T_2W MRI and DWI images while still maintaining weight sharing. The dilated heads in this model only included the DWI and ADC channels. This was performed to investigate the impact of DWI input channels on the overall contextual learning, see Figure 1 (multi-head model 2).

Finally, in the third experiment, we employed a multi-head encoding strategy with no weight sharing between the T_2W and DWI heads. Similar to the second model, we applied dilated convolutions exclusively to the DWI images to facilitate independent contextual learning and reduce boundary attention. However, this architecture included an additional concatenation layer followed by a convolutional layer for dimensionality reduction and feature summation with the T_2W head, see Figure 1 (multi-head model 3).

2.3 Image Pre-processing and Implementation Details

Prior to training, all mpMRI images were resampled to an in-plane resolution of 0.6×0.6 mm^2, which was the most common T_2W MRI resolution in the dataset (85%), and slice thickness of 4mm. Bilinear interpolation was applied for resampling T_2W and b1000 DWI images, as it allows for smooth intensity transitions, preserving the details within the images. On the other hand, ADC images and contours were resampled using the nearest neighbor interpolation method. This method was chosen for its ability to retain the original discrete values of the images, which is crucial for ADC maps due to their quantitative nature, and for contours as they represent categorical labels or boundaries in segmentation tasks. Each channel was independently normalized to a mean of zero and unit variance. Finally, the dataset was randomly split into 157, 25, and 25 patients for training, validation, and testing, respectively.

During training, sub-volumes of size $256\times256\times16$ were extracted stochastically from the training data, ensuring that each patch contained at least one annotated tumor slice. Random data augmentation operations, such as intensity shifting, scaling, and cropping, were applied to improve network generalizability. The models were trained for 100,000 iterations using the Dice loss function, which outperformed the combined Dice and cross-entropy and Tversky [24] losses during the initial experiments on input channels. The Adam optimizer with an initial learning rate of 1e-4 and weight decay of 1e-5 was used, and a cosine annealing learning rate scheduler was employed after each epoch. Validation was performed after each epoch, based on the Dice scores of whole image volumes, and the best performing weights were saved. Volumetric segmentations were generated using a sliding window algorithm with a 75% overlap between adjacent patches. The models were evaluated using the Dice similarity coefficient (DSC), 95$^{\text{th}}$ percentile Hausdorff distance (HD), mean surface distance (MSD), and percentage relative volume similarity metrics [25]. PyTorch and Monai [26] DL libraries were used for all implementations.

2.4 Channel Sensitivity Analysis and Visualization

To assess the significance of individual channels in our models, we conducted a channel sensitivity analysis using sequential channel dropout. By setting each channel to zero one at a time, we compared the segmentation results obtained from the baseline multi-channel and proposed multi-head models to those achieved with no channel dropout. We employed the same quantitative metrics utilized in our previous analyses to perform a comprehensive comparison. To gain a more nuanced understanding of the importance of channels in our models, we employed a 3D version of Gradient-weighted Class Activation Mapping (GRAD-CAM) [27]. This technique was utilized to generate saliency maps in the penultimate layers of our models, which highlighted the most relevant regions for segmentation. The

application of this technique on the center-cropped patches extracted from the test image volumes provided a detailed and insightful visualization of the channel-wise feature importance.

3 Results

The baseline multi-channel model was evaluated on various input channels and loss functions. Multi-channel input trained with Dice loss achieved the best mean segmentation performance in terms of DSC across all test cases, with consistent results across input channels. The average DSC values for multi-channel (T_2W, b1000 DWI, ADC) using Dice, combined Dice and cross-entropy, and Tversky losses were 0.672, 0.661, and 0.664, respectively (Figure 2).

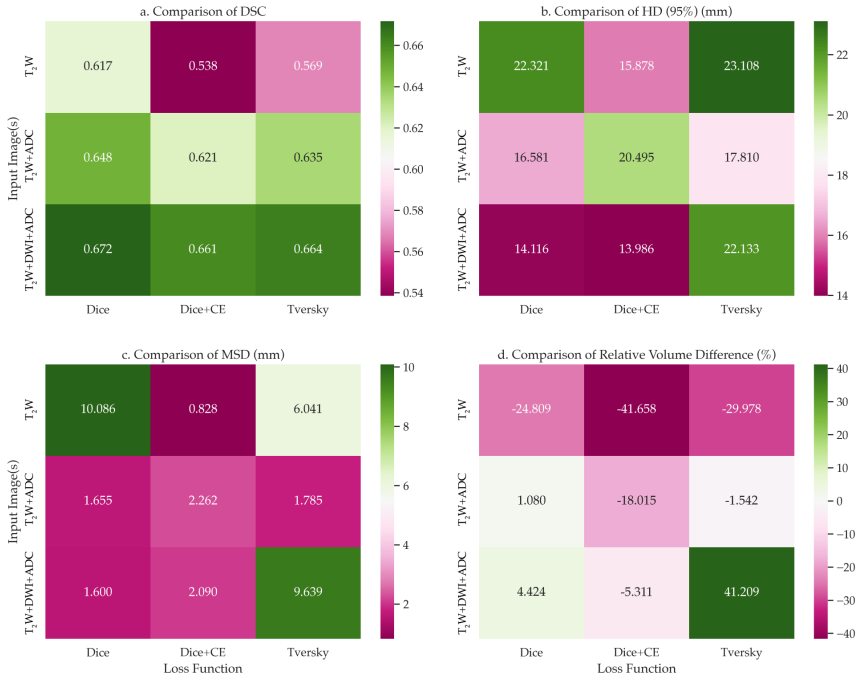

Figure 2: Heatmaps of mean a. Dice similarity coefficient (DSC), b. 95th percentile Hausdorff distance (HD), c. mean surface distance (MSD), and d. relative percentage volume difference for multi-channel residual U-Net model trained across different input images and loss functions from the test data. The model trained on all T_2W, b1000 DWI, and ADC channels, and with Dice loss achieved the best overall segmentation performance across all experiments.

The comparison of segmentations obtained from the baseline multi-channel and the proposed multi-head models revealed that multi-head model 3 exhibited superior performance across the quantitative metrics analyzed (Figure 3a-d). Specifically, the median DSC values for the multi-channel model, multi-head model 1, multi-head model 2, and multi-head model 3 were 0.788 (confidence interval (CI), 0.568–0.776), 0.805 (CI, 0.538-0.769), 0.796 (CI, 0.537-0.776), and 0.823 (CI, 0.595-0.797), respectively (Figure 3a). However, the performance differences between the proposed multi-head models were not significantly different compared with the multi-channel model ($p>0.05$). On average, all models underestimated tumor volume compared with the contours drawn by the clinician, with the median relative percentage volume differences for each model of -14.4%, -18.9%, -9.7%, and -12.0%, respectively (Figure 3d). The multi-head model 3 demonstrated the best quantitative scores compared to the other experimental architectures, therefore, the segmentation contours predicted by this model were compared with those obtained from the baseline multi-channel model (Figure 4).

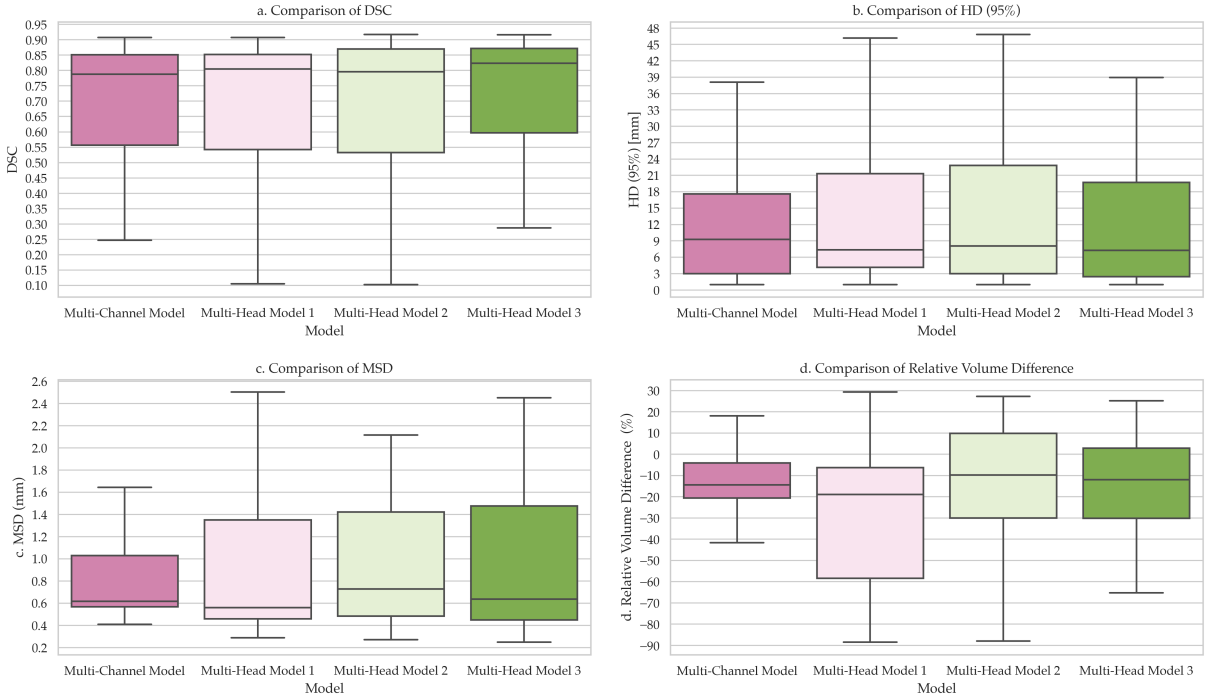

Figure 3: Comparison of segmentation performance based on a. Dice similarity coefficient (DSC), b. 95th percentile Hausdorff distance (HD), c. mean surface distance (MSD), and d. relative percentage volume difference between the baseline multi-channel model and three variations of the dilated multi-head model. Overall, the multi-head model with dilated convolutions and separate DWI/ADC feature aggregation (multi-head model 3) achieved the best performance across all models.

The channel sensitivity analysis conducted between the multi-channel and proposed multi-head model indicated that the multi-head model's tumor segmentation performance significantly suffered when the ADC channel was removed (Figure 5). Moreover, the saliency maps generated from both models revealed that b1000 DWI images had a relatively minor impact on the overall tumor segmentation performance for larger tumor volumes, while T_2W and ADC images were more crucial (see Figure 6, test cases 1 and 2). Conversely, for smaller and more challenging tumor masses, the absence of ADC values had a more pronounced adverse effect on the final outcome (see Figure 6, test cases 3-5).

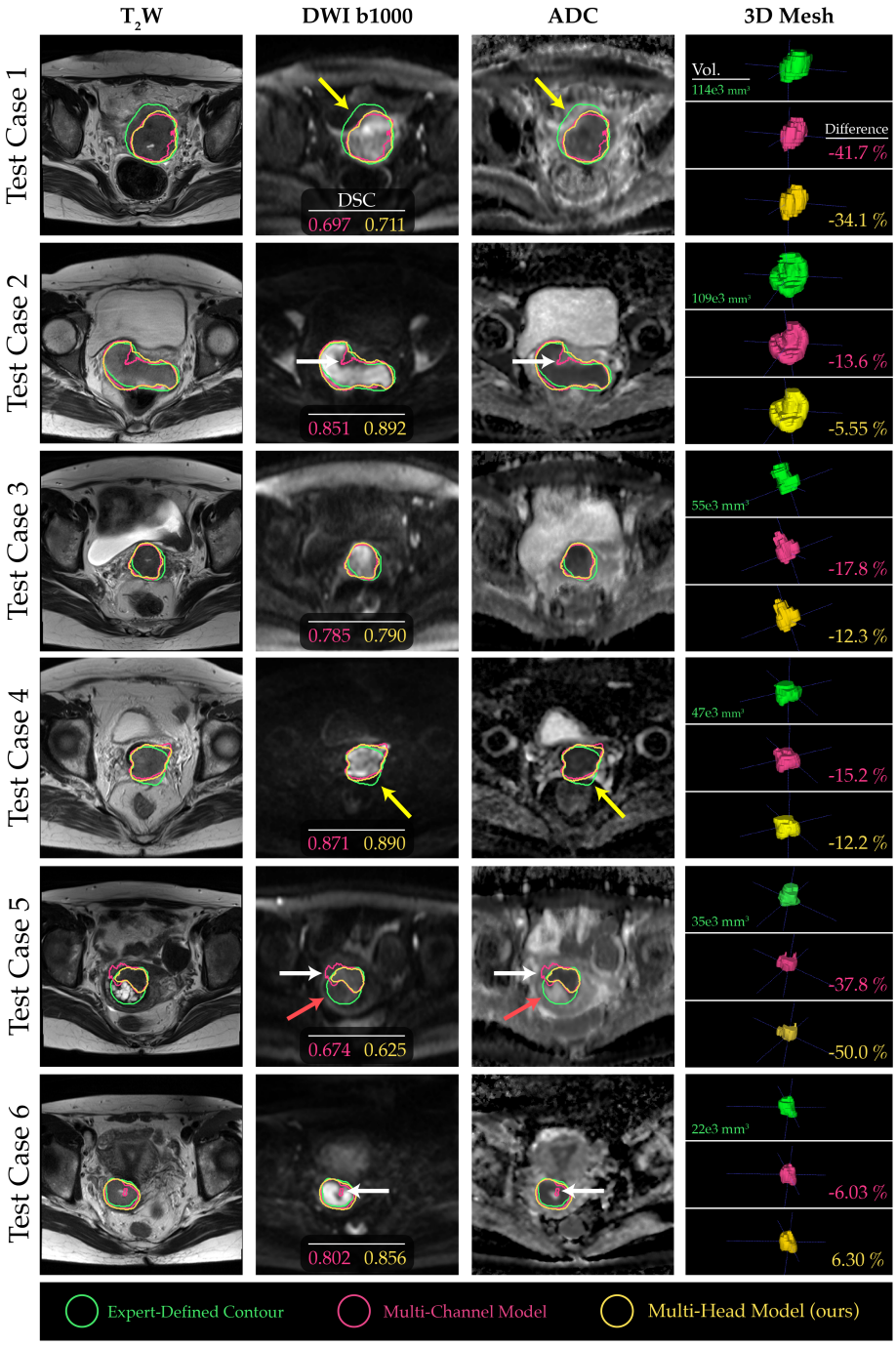

Figure 4: Comparative evaluation of the baseline multi-channel and proposed multi-head models for 6 test cases, arranged in descending order of tumor size. The yellow arrows indicate regions where distortion in DWI and subjectivity in tumor location make contour propagation from T_2W images challenging. Conversely, the white arrows highlight regions where the proposed model performed better by capturing boundaries and contextual information compared to the baseline multi-channel model. The red arrows highlight tumor regions within the ground truth contours that do not exhibit strong impeded diffusion, thus remaining undetected by the DL models.

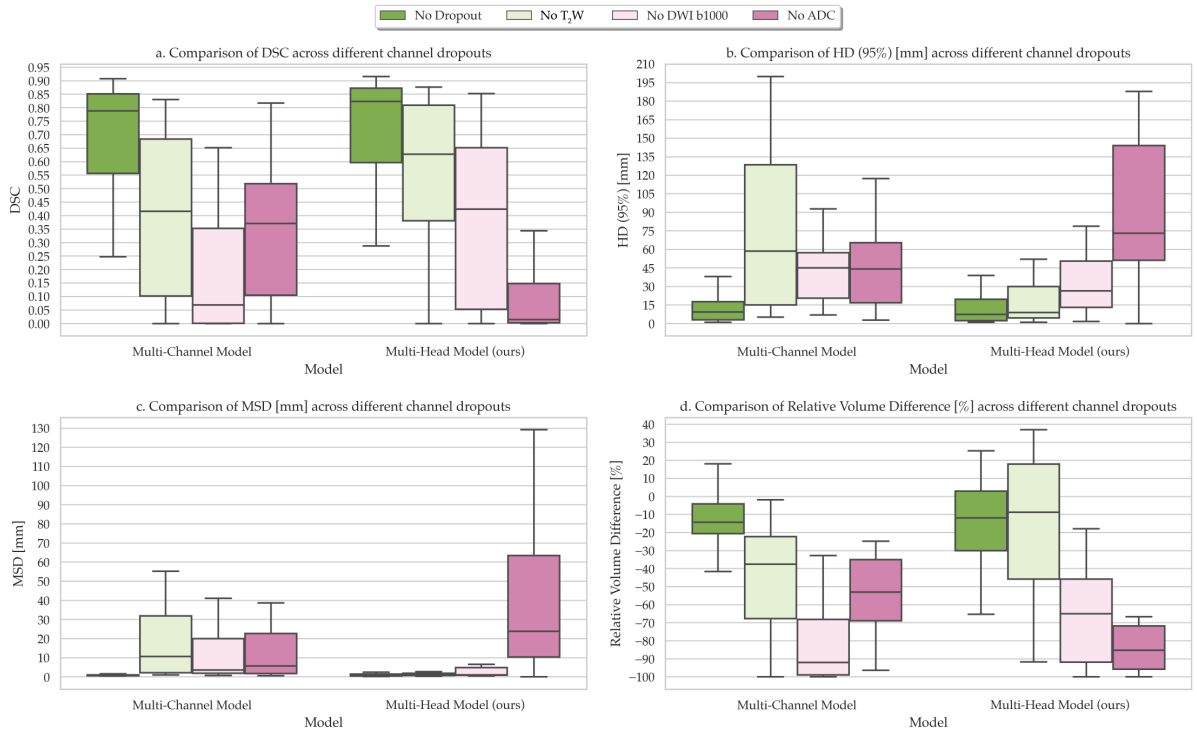

Figure 5: Comparison of the sensitivity of the multi-channel and proposed multi-head models to different input channels based on quantitative metrics, including a. Dice similarity coefficient (DSC), b. 95th percentile Hausdorff distance (HD), c. mean surface distance (MSD), and d. relative percentage volume difference. Our channel dropout analysis revealed a strong dependence of the proposed multi-head model on the ADC channel, indicating its importance in achieving accurate segmentation performance.

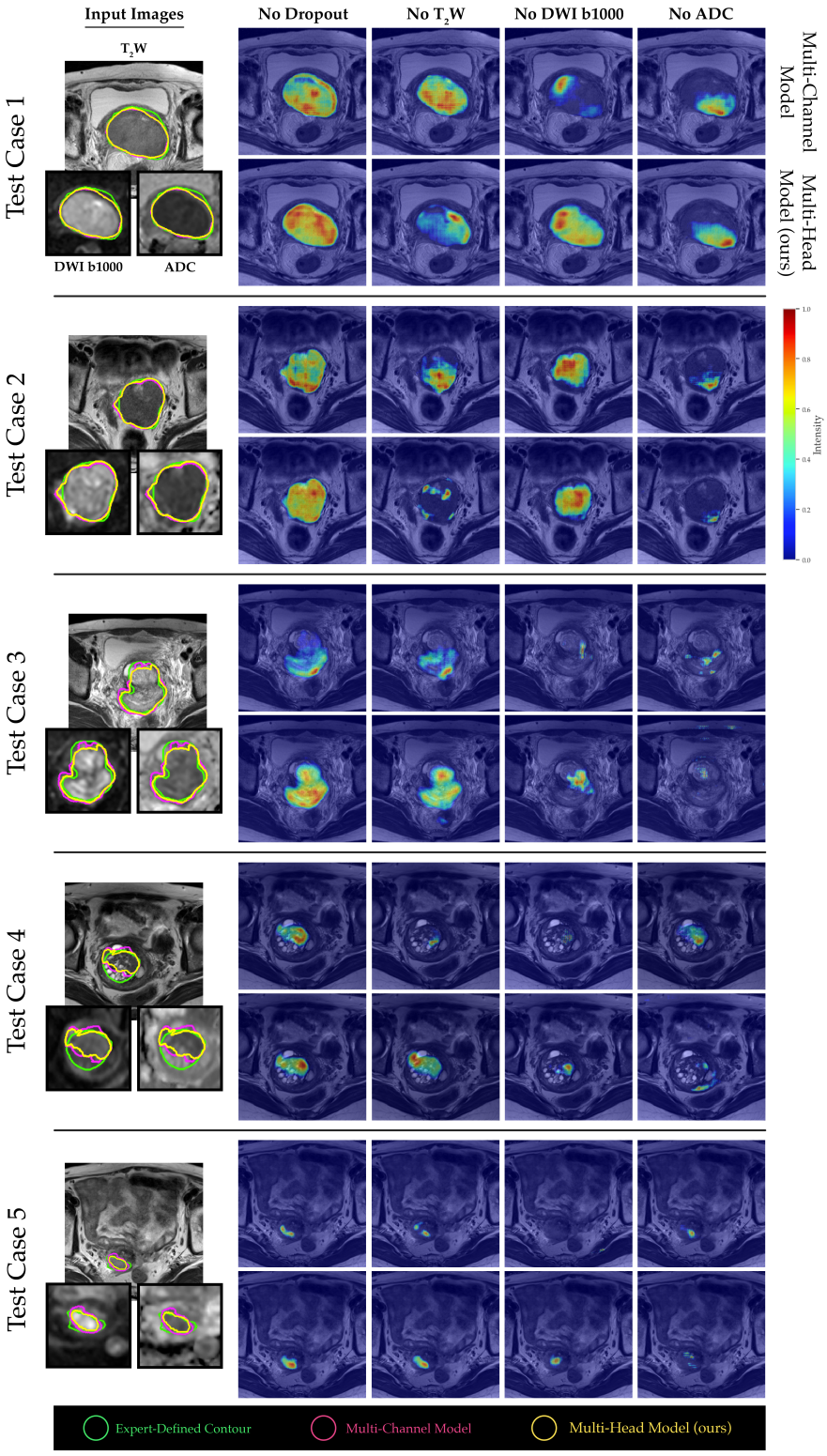

Figure 6: The normalized 3D GRAD-CAM saliency maps generated from the penultimate layer of models, highlighting the most relevant regions for segmentation under different channel dropout conditions at test time. To improve visualization, the b1000 DWI and ADC images for smaller tumors were scaled.

4 Discussion

DWI is a critical functional imaging technique for the detection and localization of tumors. This is particularly evident on ADC maps, where regions depicting impeded water molecule diffusion are indicative of increased cell density, often signifying a more aggressive disease [28]. However, using DWI and ADC maps in conjunction with T_2W MRI sequences presents several challenges, such as voxel misalignment due to distortion and soft-tissue deformations between scans, variations in tumor delineations between the two modalities and the absence of standardized protocols for mpMRI. In this study, we proposed a multi-head framework that utilizes both DWI (including ADC) and T_2W MRI for cervical cancer segmentation, a process well-suite for biomarker extraction. Our framework includes separate encoding heads that extract contextual information about tumors using dilated (or atrous) convolutions and shared residual connections. We have demonstrated that our technique provides more robust and boundary-aware segmentation of cervical tumors when compared with the baseline multi-channel architecture used in previous studies [17, 20]. Our findings using the multi-channel training approach are comparable to previous reports on segmentation of cervical tumors on multiparametric MRI [14, 17, 20]. However, it is challenging to make direct comparisons of our results due to the lack of public databases for cervical cancer segmentation on MRI [11] and the use of different datasets.

Dilated convolutions are a crucial component of several successful segmentation architectures, including DeepLabv3+ [29], DeepLab [30], residual enhanced U-Net and atrous convolution (AtResU-Net) [31], and 3D deeply supervised fully-convolutional network with concatenated atrous convolution (3D DSA-FCN) [32]. While most of these techniques utilize dilated convolutions throughout their architecture's encoding steps, we propose a multi-head framework that uses these operations for separate contextual and representational learning in DWI and ADC images only for the first block of the encoder. This approach ensures that the training parameters are not substantially increased compared with baseline multi-channel architectures, and the model is easier to interpret with conventional methods for future explainability studies. Moreover, lighter networks are better suited for online MR-guided treatments, where segmentation and planning are performed live on the scan of the day before radiation treatment [33], and speed is of the essence. In this study, we trained our models using anisotropic sub-volumes to maintain a greater focus on the plane of acquisition (axial) for 2D MRI. However, our method can be extended to 3D MRI scans, which are more commonly used for radiation therapy.

Channel sensitivity and saliency mapping of our experimental model indicated that our algorithm was more sensitive to DWI and, particularly, ADC maps, which potentially make it more robust to changes in acquisition protocol on MRI scanners. This approach could also serve as a strategy for more generalizable and cross-disease detection models [34]. However, this dependence on DWI, as demonstrated in this study, may result in underestimation of the predicted tumor volume for malignancies with heterogeneous tumor mass diffusion. Moreover, the subjectivity associated with inter-operator variability presents another drawback, with more reliable segmentations only attainable through the use of consensus contours. The decision to include specific areas within the ground truth contour of the tumor is a discretionary choice made by the clinical expert annotating the images, a decision that relies heavily on their professional training and experience. Hence, future studies should aim to employ consensus ground truth contours and evaluate the segmentation outcome through a number of expert human reader assessments to ensure the accuracy and reliability of the results for clinical decision-making.

In conclusion, our proposed multi-head framework that combines DWI, ADC and T_2W MRI for cervical cancer segmentation has demonstrated improved accuracy and robustness compared to conventional multi-channel architectures. The use of dilated convolutions in only the first block of the encoder improves contextual learning with no significant parameter increase compared with conventional U-Net models. However, the dependence on DWI and subjectivity in inter-operator variability are potential limitations that need to be addressed in future studies through the use of

consensus ground truth contours and expert human reader assessments. Overall, our approach has the potential to improve clinical decision-making for not only cervical cancer but also other pelvic malignancies.

Acknowledgments

This study represents independent research funded by the National Institute for Health and Care Research (NIHR) Biomedical Research Centre and the Clinical Research Facility in Imaging at The Royal Marsden NHS Foundation Trust and The Institute of Cancer Research, London. The views expressed are those of the author(s) and not necessarily those of the NIHR or the Department of Health and Social Care. Gigin Lin received research funding from the Ministry of Science and Technology Taiwan (MOST 110-2628-B-182A-018).

References

[1] Kaori Togashi, Kazumasa Nishimura, Tadashi Sagoh, Shunsuke Minami, Satoshi Noma, Ichiro Fujisawa, Yoshihisa Nakano, Junji Konishi, H Ozasa, and I Konishi. Carcinoma of the cervix: staging with mr imaging. *Radiology*, 171(1):245–251, 1989.

[2] John A Green, John M Kirwan, Jayne F Tierney, Paul Symonds, Lydia Fresco, Mandy Collingwood, and Christopher J Williams. Survival and recurrence after concomitant chemotherapy and radiotherapy for cancer of the uterine cervix: a systematic review and meta-analysis. *The lancet*, 358(9284):781–786, 2001.

[3] Julianne M Pollard, Zhifei Wen, Ramaswamy Sadagopan, Jihong Wang, and Geoffrey S Ibbott. The future of image-guided radiotherapy will be mr guided. *The British journal of radiology*, 90(1073):20160667, 2017.

[4] Dow-Mu Koh and Harriet C Thoeny. *Diffusion-weighted MR imaging: applications in the body*. Springer Science & Business Media, 2010.

[5] Soichiro Yoshida, Taro Takahara, Thomas C Kwee, Yuma Waseda, Shuichiro Kobayashi, and Yasuhisa Fujii. Dwi as an imaging biomarker for bladder cancer. *American Journal of Roentgenology*, 208(6):1218–1228, 2017.

[6] Chie Tsuruta, Kenji Hirata, Kohsuke Kudo, Naoya Masumori, and Masamitsu Hatakenaka. Dwi-related texture analysis for prostate cancer: Differences in correlation with histological aggressiveness and data repeatability between peripheral and transition zones. *European radiology experimental*, 6:1–12, 2022.

[7] Toru Higaki, Yuko Nakamura, Fuminari Tatsugami, Yoko Kaichi, Motonori Akagi, Yuij Akiyama, Yasutaka Baba, Makoto Iida, and Kazuo Awai. Introduction to the technical aspects of computed diffusion-weighted imaging for radiologists. *Radiographics*, 38(4):1131–1144, 2018.

[8] Sahar Mahmoud Abd elsalam, Omnia Mokhtar, Lamia Adel, Reda Hassan, Manal Ibraheim, and Amro Kamal. Impact of diffusion weighted magnetic resonance imaging in diagnosis of cervical cancer. *Egyptian Journal of Radiology and Nuclear Medicine*, 51:1–8, 2020.

[9] Leslee E Subak, Hedvig Hricak, C Bethan Powell, Eouisa Azizi, and Jeffrey L Stern. Cervical carcinoma: computed tomography and magnetic resonance imaging for preoperative staging. *Obstetrics & Gynecology*, 86(1):43–50, 1995.

[10] Paul B Romesser, Neelam Tyagi, and Christopher H Crane. Magnetic resonance imaging-guided adaptive radiotherapy for colorectal liver metastases. *Cancers*, 13(7):1636, 2021.

[11] Reza Kalantar, Gigin Lin, Jessica M Winfield, Christina Messiou, Susan Lalondrelle, Matthew D Blackledge, and Dow-Mu Koh. Automatic segmentation of pelvic cancers using deep learning: state-of-the-art approaches and challenges. *Diagnostics*, 11(11):1964, 2021.

[12] Bastien Rigaud, Brian M Anderson, H Yu Zhiqian, Maxime Gobeli, Guillaume Cazoulat, Jonas Söderberg, Elin Samuelsson, David Lidberg, Christopher Ward, Nicolette Taku, et al. Automatic segmentation using deep learning to enable online dose optimization during adaptive radiation therapy of cervical cancer. *International Journal of Radiation Oncology* Biology* Physics*, 109(4):1096–1110, 2021.

[13] Chen-Ying Ma, Ju-Ying Zhou, Xiao-Ting Xu, Jian Guo, Miao-Fei Han, Yao-Zong Gao, Hui Du, Johannes N Stahl, and Jonathan S Maltz. Deep learning-based auto-segmentation of clinical target volumes for radiotherapy treatment of cervical cancer. *Journal of Applied Clinical Medical Physics*, 23(2):e13470, 2022.

[14] Bin Wang, Yuanyuan Zhang, Chunyan Wu, Fen Wang, et al. Multimodal mri analysis of cervical cancer on the basis of artificial intelligence algorithm. *Contrast Media & Molecular Imaging*, 2021, 2021.

[15] Pengyue Lu, Faming Fang, He Zhang, Lei Ling, and Keqin Hua. Augms-net: Augmented multiscale network for small cervical tumor segmentation from mri volumes. *Computers in Biology and Medicine*, 141:104774, 2022.

[16] Fatemeh Zabihollahy, Akila N Viswanathan, Ehud J Schmidt, and Junghoon Lee. Fully automated segmentation of clinical target volume in cervical cancer from magnetic resonance imaging with convolutional neural network. *Journal of applied clinical medical physics*, 23(9):e13725, 2022.

[17] Yu-Chun Lin, Chia-Hung Lin, Hsin-Ying Lu, Hsin-Ju Chiang, Ho-Kai Wang, Yu-Ting Huang, Shu-Hang Ng, Ji-Hong Hong, Tzu-Chen Yen, Chyong-Huey Lai, et al. Deep learning for fully automated tumor segmentation and extraction of magnetic resonance radiomics features in cervical cancer. *European radiology*, 30:1297–1305, 2020.

[18] Yosuke Kano, Hitoshi Ikushima, Motoharu Sasaki, and Akihiro Haga. Automatic contour segmentation of cervical cancer using artificial intelligence. *Journal of Radiation Research*, 62(5):934–944, 2021.

[19] SA Yoganathan, Siji Nojin Paul, Satheesh Paloor, Tarraf Torfeh, Suparna Halsnad Chandramouli, Rabih Hammoud, and Noora Al-Hammadi. Automatic segmentation of magnetic resonance images for high-dose-rate cervical cancer brachytherapy using deep learning. *Medical Physics*, 49(3):1571–1584, 2022.

[20] Erlend Hodneland, Satheshkumar Kaliyugarasan, Kari Strøno Wagner-Larsen, Njål Lura, Erling Andersen, Hauke Bartsch, Noeska Smit, Mari Kyllesø Halle, Camilla Krakstad, Alexander Selvikvåg Lundervold, et al. Fully automatic whole-volume tumor segmentation in cervical cancer. *Cancers*, 14(10):2372, 2022.

[21] Takeshi Yoshizako, Rika Yoshida, Hiroya Asou, Megumi Nakamura, and Hajime Kitagaki. Comparison between turbo spin-echo and echo planar diffusion-weighted imaging of the female pelvis with 3t mri. *Acta Radiologica Open*, 10(2):2058460121994737, 2021.

[22] Francisco Donato Jr, Daniel N Costa, Qing Yuan, Neil M Rofsky, Robert E Lenkinski, and Ivan Pedrosa. Geometric distortion in diffusion-weighted mr imaging of the prostate—contributing factors and strategies for improvement. *Academic radiology*, 21(6):817–823, 2014.

[23] Olaf Ronneberger, Philipp Fischer, and Thomas Brox. U-net: Convolutional networks for biomedical image segmentation. In *Medical Image Computing and Computer-Assisted Intervention–MICCAI 2015: 18th International Conference, Munich, Germany, October 5-9, 2015, Proceedings, Part III 18*, pages 234–241. Springer, 2015.

[24] Amos Tversky. Features of similarity. *Psychological review*, 84(4):327, 1977.

[25] Abdel Aziz Taha and Allan Hanbury. Metrics for evaluating 3d medical image segmentation: analysis, selection, and tool. *BMC medical imaging*, 15(1):1–28, 2015.

[26] M Jorge Cardoso, Wenqi Li, Richard Brown, Nic Ma, Eric Kerfoot, Yiheng Wang, Benjamin Murrey, Andriy Myronenko, Can Zhao, Dong Yang, et al. Monai: An open-source framework for deep learning in healthcare. *arXiv preprint arXiv:2211.02701*, 2022.

[27] Ramprasaath R Selvaraju, Michael Cogswell, Abhishek Das, Ramakrishna Vedantam, Devi Parikh, and Dhruv Batra. Grad-cam: Visual explanations from deep networks via gradient-based localization. In *Proceedings of the IEEE international conference on computer vision*, pages 618–626, 2017.

[28] Patrick Z McVeigh, Aejaz M Syed, Michael Milosevic, Anthony Fyles, and Masoom A Haider. Diffusion-weighted mri in cervical cancer. *European radiology*, 18:1058–1064, 2008.

[29] Liang-Chieh Chen, Yukun Zhu, George Papandreou, Florian Schroff, and Hartwig Adam. Encoder-decoder with atrous separable convolution for semantic image segmentation. In *Proceedings of the European conference on computer vision (ECCV)*, pages 801–818, 2018.

[30] Liang-Chieh Chen, George Papandreou, Iasonas Kokkinos, Kevin Murphy, and Alan L Yuille. Deeplab: Semantic image segmentation with deep convolutional nets, atrous convolution, and fully connected crfs. *IEEE transactions on pattern analysis and machine intelligence*, 40(4):834–848, 2017.

[31] Nisarg A Shah, Divij Gupta, Romil Lodaya, Ujjwal Baid, and Sanjay Talbar. Colorectal cancer segmentation using atrous convolution and residual enhanced unet. In *Computer Vision and Image Processing: 5th International Conference, CVIP 2020, Prayagraj, India, December 4-6, 2020, Revised Selected Papers, Part I 5*, pages 451–462. Springer, 2021.

[32] Bo Wang, Yang Lei, Jiwoong Jason Jeong, Tonghe Wang, Yingzi Liu, Sibo Tian, Pretesh Patel, Xiaojun Jiang, Ashesh B Jani, Hui Mao, et al. Automatic mri prostate segmentation using 3d deeply supervised fcn with concatenated atrous convolution. In *Medical Imaging 2019: Computer-Aided Diagnosis*, volume 10950, pages 988–995. SPIE, 2019.

[33] Adrian L Breto, Benjamin Spieler, Olmo Zavala-Romero, Mohammad Alhusseini, Nirav V Patel, David A Asher, Isaac R Xu, Jacqueline B Baikovitz, Eric A Mellon, John C Ford, et al. Deep learning for per-fraction automatic segmentation of gross tumor volume (gtv) and organs at risk (oars) in adaptive radiotherapy of cervical cancer. *Frontiers in oncology*, 12, 2022.

[34] Yu-Chun Lin, Yenpo Lin, Yen-Ling Huang, Chih-Yi Ho, Hsin-Ju Chiang, Hsin-Ying Lu, Chun-Chieh Wang, Jiun-Jie Wang, Shu-Hang Ng, Chyong-Huey Lai, et al. Generalizable transfer learning of automated tumor segmentation from cervical cancers toward a universal model for uterine malignancies in diffusion-weighted mri. *Insights into Imaging*, 14(1):14, 2023.